

# A genetic algorithm for the non-parametric inversion of strong lensing systems

J. Liesenborgs<sup>1\*</sup>, S. De Rijcke<sup>2†</sup> and H. Dejonghe<sup>2</sup>

<sup>1</sup> *Expertisecentrum voor Digitale Media, Universiteit Hasselt, Wetenschapspark 2, B-3590, Diepenbeek, Belgium*

<sup>2</sup> *Sterrenkundig Observatorium, Universiteit Gent, Krijgslaan 281, S9, B-9000, Gent, Belgium*

## ABSTRACT

We present a non-parametric technique to infer the projected-mass distribution of a gravitational lens system with multiple strong-lensed images. The technique involves a dynamic grid in the lens plane on which the mass distribution of the lens is approximated by a sum of basis functions, one per grid cell. We used the projected mass densities of Plummer spheres as basis functions. A genetic algorithm then determines the mass distribution of the lens by forcing images of a single source, projected back onto the source plane, to coincide as well as possible. Averaging several tens of solutions removes the random fluctuations that are introduced by the reproduction process of genomes in the genetic algorithm and highlights those features common to all solutions. Given the positions of the images and the redshifts of the sources and the lens, we show that the mass of a gravitational lens can be retrieved with an accuracy of a few percent and that, if the sources sufficiently cover the caustics, the mass distribution of the gravitational lens can also be reliably retrieved. A major advantage of the algorithm is that it makes full use of the information contained in the radial images, unlike methods that minimise the residuals of the lens equation, and is thus able to accurately reconstruct also the inner parts of the lens.

**Key words:** gravitational lensing – methods: data analysis – dark matter – galaxies: clusters: general

## 1 INTRODUCTION

The deflection of light caused by a gravitational lens and the amplifying and distorting effect thereof on the images of background sources, provide us with a means to measure the total mass of the lensing object. If only, of course, that it is possible to “invert” such a lensing system, i.e. to infer the mass distribution of the lens given the positions and shapes of a set of lensed images of background sources and the redshifts of the lens and the sources. The inversion of gravitational lensing systems is interesting in its own right, since it puts constraints on the spatial dark matter distribution of the lensing objects and thus helps constrain dark matter physics (Navarro et al. 2004; Diemand, Moore, Stadel 2004), but it may also contribute to cosmology. Good reconstructions of lensing systems may help to constrain the density parameter and the redshift evolution of the dark energy (Yamamoto et al. 2001; Soucail et al. 2004; Meneghetti et al. 2005).

The use of the gravitational lensing effect to measure masses of point-mass lenses (or “stars”) was envisaged by Refsdal (1964) and Liebes (1964). The idea of using simple parametric models for extended lenses, such as galaxies or clusters of galaxies, can be traced back to Dyer & Roeder (1980), who use a King model to estimate the mass distribution of the galaxy that produces the two images of QSO 0957+561A, B. Since then a host of parametric inversion methods has been developed and applied to observed strong lensing systems, such as the ring cycle method of Kochanek et al. (1989) or the maximum entropy method of Wallington et al. (1994). Kneib et al. (1993) fitted a bimodal lensing potential, constructed from two elliptical pseudo-isothermal potentials, images of the cluster A370, obtained from the ground under excellent seeing conditions. More elaborate parametric models for lensing clusters associate a simple mass distribution, e.g. a power-law of

\* Corresponding author: jori.liesenborgs@uhasselt.be

† Postdoctoral Fellow of the Fund for Scientific Research - Flanders (Belgium)(F.W.O)

radius, to each galaxy and to the cluster as a whole. The many parameters that define the lens model are then determined by a  $\chi^2$  fit to the observed images (Tyson, Kochanski, Dell’Antonio 1998). Brewer & Lewis (2005) suggest using a gravitational lens as a cosmic magnifying glass to recover structural details about distant sources. These authors assume a parametric form for the lens mass distribution and use a genetic algorithm to non-parametrically reconstruct the surface brightness distribution of the source. If only a few sources are being lensed or if the sources do not sufficiently cover the caustics, parametric methods are clearly the preferred approach.

However, the multitude of arcs and distorted images visible in massive clusters (e.g. Soucail et al. 1987; Lavery & Henry 1988), which are observed routinely now at high spatial resolution with the Hubble Space Telescope (e.g. Broadhurst et al. 2005), contain a wealth of information and call for more flexible and model independent inversion methods. Using the pixelation method (Saha & Williams 1997; AbdelSalam, Saha, Williams 1998), the lens plane is divided into a static grid. The mass in each grid cell and the source positions are estimated so as to construct a solution that best reproduces the observed image positions, subject to regularizing constraints that ensure a smooth mass distribution for the lens that stays close to the luminosity distribution. Trotter, Winn, Hewitt (2000) perform a multipole-Taylor expansion of the two-dimensional lensing potential, the coefficients of which are determined by a  $\chi^2$ -fit to the observed images. In Diego et al. (2005a), a non-parametric inversion technique, called SLAP, is presented and applied to an HST image of the cluster Abell 1689 (Diego et al. 2005b; King, Clowe, Schneider 2002) that, like the pixelation method, makes use of a grid division of the mass distribution of the lens. This time, however, the grid is dynamic: it is refined iteratively where the mass density is large. Recently, Diego et al. (2005c) extended SLAP to WSLAP in order to also take into account information in the weak lensing regime. Thus, SLAP and WSLAP are fast and versatile tools for inverting observed lens systems. However, both methods assume the background galaxies to be point sources, which may lead to an over-estimation of the central mass density of the lens in order to focus the images into very compact sources and to physically implausible regions with negative mass density in the lens plane. Adding weak-lensing information alleviates the dependence of the solution on this minimization threshold. WSLAP can make use of quadratic programming to avoid unphysical negative mass densities for the lens. However, this limits the analysis to observables that are linear functions of the lens mass density, such as image positions, and does not allow to incorporate e.g. surface brightness information, which depends non-linearly on the lens mass density. Bradač et al. (2005) also used weak and strong lensing data to invert the X-ray cluster RX J1347.5–1145. Their method evaluates the gravitational potential on a non-dynamic grid. The best fitting gravitational potential is then constructed non-parametrically by minimising a  $\chi^2$  function, starting from a parametric priorsolution.

The ideal non-parametric lens inversion algorithm *(i)* should be free of any assumptions regarding the mass distribution of the lens or the luminosity distributions of the sources, *(ii)* should not depend on any prior on the lens mass distribution or any regularisation scheme that could bias the solution, *(iii)* should not produce unphysical, i.e. negative, mass densities *(iv)* should be free of any uncontrollable parameters, *(v)* should be easily extendible to any kind of data, both in the strong and weak lensing regimes, without having to change the inner workings of the algorithm or having to worry about features like continuity or differentiability of the objective function that is extremised. These conceptual issues are the main motivation for this paper, rather than computational speed.

Genetic algorithms do an excellent job at fulfilling all these constraints. In this paper, we describe and test a new non-parametric lens inversion technique. The technique makes use of a dynamic grid on which the mass distribution of the lens is approximated by a weighted sum of basis functions and of a genetic algorithm to determine the unknown weights. In the strong lensing regime, where multiple images of each source are available, the following data are offered to the algorithm: the redshifts of the sources and the lens, and the observed positions of the images. The genetic algorithm generates solutions that satisfy only one minimal constraint: the back-projected images of a single source should overlap as well as possible in the source plane.

We briefly describe the relevant background to gravitational lens systems and genetic algorithms in Section 2. The details of the inversion method are given in Sect. 3. We discuss a number of tests to which we subjected the method in Sect. 4. Finally, our conclusions are summarized in Sect. 5.

## 2 BACKGROUND

### 2.1 The lens equation

In the thin lens approximation, the lens equation relates viewing directions  $\theta$ , that are defined in the lens plane, to positions  $\beta$  in the source plane:

$$\beta(\theta) = \theta - \frac{D_{ds}}{D_s} \hat{\alpha}(\theta), \quad (1)$$

with  $\hat{\alpha}$  the deflection angle,  $D_s$  the distance between the observer and the source, and  $D_{ds}$  the distance between the lens and the source. The gravitational bending of light rays, described by the deflection angle  $\hat{\alpha}$ , depends on the viewing direction  $\theta$ ,

the mass distribution of the lens and the distance between the lens and the observer. Here and in the following, distances should be interpreted as angular-diameter distances. For simplicity, we will adopt a standard CDM cosmology, with a matter density  $\Omega = 1$  and a Hubble parameter  $H_0 = 70 \text{ km s}^{-1} \text{ Mpc}^{-1}$ , in which the angular-diameter distance between an observer at redshift  $z_1$  and a source at redshift  $z_2$  is given by

$$D(z_1, z_2) = \frac{2c}{H_0} \frac{1}{1+z_2} \left( \frac{1}{\sqrt{1+z_1}} - \frac{1}{\sqrt{1+z_2}} \right). \quad (2)$$

We will always assume that the redshifts of the lens and of the source(s) are known to the observer. The lens equation projects the images back onto their respective sources in the source plane. When a gravitational lens produces multiple images of a single source, one can use the lens equation to find, for each image, the corresponding region in the source plane. Since all images correspond to a single source, all back-projected images have to coincide.

## 2.2 The Plummer lens

We first describe the gravitational lens effect caused by a Plummer sphere (Plummer 1911) at a distance  $D_d$  from the observer. The projected density distribution of a Plummer sphere with total mass  $M$  and angular scale-length  $\theta_P$  as a function of angular distance  $\theta$  is given by

$$\Sigma(\theta) = \frac{M}{\pi D_d^2} \frac{\theta_P^2}{(\theta^2 + \theta_P^2)^2}. \quad (3)$$

This mass distribution leads to the following lens equation:

$$\beta(\theta) = \theta - \frac{D_{ds}}{D_s D_d} \frac{4GM}{c^2} \frac{\theta}{\theta^2 + \theta_P^2} \quad (4)$$

if the coordinate system in the lens plane is centered on the Plummer sphere.

As a first step towards inverting a given lens system, we write the (unknown) projected mass distribution of the lens as a sum of Plummer mass distributions, of the form given by eq. (3). We chose the Plummer mass distribution as basis function because it is well-behaved at all radii and yields a finite total mass. The deflection angle is then simply the sum of the deflection angles caused by each individual Plummer distribution. For  $N$  individual Plummer lenses, this yields the following lens equation:

$$\beta(\theta) = \theta - \frac{D_{ds}}{D_s D_d} \frac{4G}{c^2} \sum_{i=1}^N \frac{\theta - \theta_{s,i}}{|\theta - \theta_{s,i}|^2 + \theta_{P,i}^2} M_i, \quad (5)$$

with  $\theta_{s,i}$  the position of the centre of a Plummer distribution in the lens plane,  $M_i$  its mass, and  $\theta_{P,i}$  its angular scale-length.

A given set of  $R$  points in the lens plane,  $\theta_k$ ,  $k = 1 \dots R$ , is related to a corresponding set of  $R$  points in the source plane by a matrix equation (Diego et al. 2005a). Indeed, let  $\Theta$  be a vector of length  $2R$ , containing the coordinates of the points in the image plane, in which  $x$  and  $y$  components alternate. Similarly,  $B$  is a vector of length  $2R$  which will contain the coordinates of the corresponding points in the source plane. The masses  $M_i$  of the Plummer distributions that make up the mass distribution of the lens are stored in an  $N$  dimensional column vector  $M$ . The lens equation can then be rewritten as

$$B = \Theta - \gamma M, \quad (6)$$

with  $\gamma$  a  $2R \times N$  matrix whose components are given by:

$$\begin{aligned} \gamma_{2k-1,l} &= \frac{D_{ds}}{D_d D_s} \frac{4G}{c^2} \frac{(\theta_k - \theta_{s,l})_x}{|\theta_k - \theta_{s,l}|^2 + \theta_{P,l}^2} \\ \gamma_{2k,l} &= \frac{D_{ds}}{D_d D_s} \frac{4G}{c^2} \frac{(\theta_k - \theta_{s,l})_y}{|\theta_k - \theta_{s,l}|^2 + \theta_{P,l}^2}. \end{aligned} \quad (7)$$

The problem of inverting a gravitational lens system is thus transformed into the problem of finding the vector  $M$ , given the matrices  $\Theta$  and  $\gamma$ .

## 2.3 Genetic algorithms

With genetic algorithms, one tries to breed good solutions to a given problem. A central concept is the genome, which is an encoded representation of a possible solution. Usually, the genome will encode the parameters of a specific model. For a particular genome, there has to be some kind of measure of how adequate it fits the data. This value is usually called the fitness of the genome. The algorithm starts with a random set of genomes: the population. From this population, a new one will be created using the following procedure:

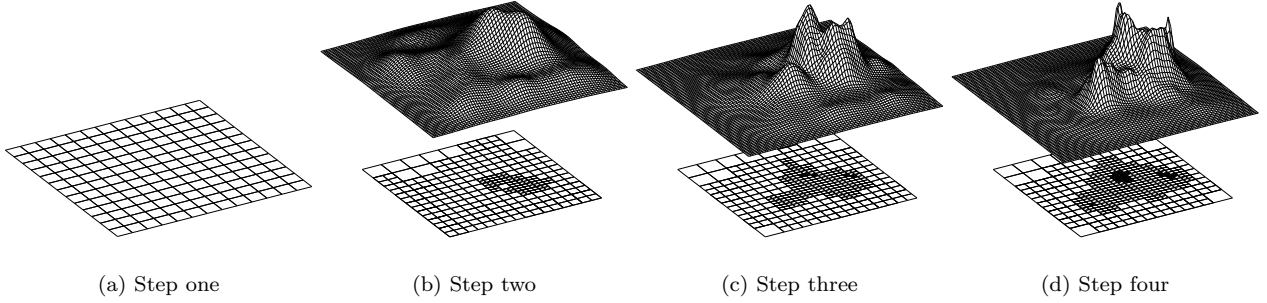


**Figure 1.** The use of a dynamic grid. The grid spacing is refined in those regions where individual grid cells contain a large fraction of the total mass of the lens or where the projected-density gradients are large.

- For each genome, the fitness is calculated.
- A new set of genomes is created by combining and copying genomes of the current population. Selection of genomes in this reproduction step should favor genomes with a better fitness.
- Finally, mutations are introduced in the new population to ensure genetic variety.

When creating the new population, the best genome is often copied without mutations. This approach is often referred to as elitism and ensures that the best member of the new population will perform at least as well as the fittest member of the old population. Thus, generation after generation, one tries to breed increasingly better solutions to a problem. A complete overview of genetic programming techniques can be found in Koza (1992).

### 3 THE INVERSION METHOD

In the following, we discuss two key features of our inversion method: the use of a dynamic grid in the lens plane on which the Plummer lenses are positioned (which defines the matrix  $\gamma$ ) and the genetic algorithm employed to breed the best approximation to the projected mass distribution of the lens (i.e., the vector  $M$ ).

#### 3.1 The dynamic grid

The procedure starts with a square grid, large enough to encompass the projected mass density of the lens. At first, this area is uniformly subdivided in square grid cells. At the centre of each grid cell, a Plummer mass distribution is positioned. The width of each Plummer distribution is set proportional to the side of its grid cell. We tested which proportionality factor allows to best reproduce a wide range of mass densities and found that a value of 1.7 yields a good trade-off between smoothness and dynamic range. The same scale factor was subsequently used in our lens inversion simulations. The genetic algorithm (see subsection 3.2) then breeds, for this given grid, the best solution  $M$ . Given this first approximation of the total mass density, a new grid is constructed by further subdividing grid cells that contain a large fraction of the total mass or that reside in areas with large density gradients. This way, the new grid will allow a better approximation of the mass density, without wasting resources on areas which contain little mass or detail. With each cell of this new grid a Plummer distribution is associated and the individual masses are determined by the genetic algorithm, as before. In our implementation, this procedure of refining the grid is repeated unless the number of grid cells exceeds one thousand. Fig. 1 illustrates the procedure. At first, a uniform grid is used. With this grid, a first estimate of the distribution is found and this is used to create a new grid. The figure shows a few additional mass density estimates on which new grids are based.

#### 3.2 The genetic algorithm

##### 3.2.1 Genome and fitness

The goal of the genetic algorithm is to determine good values for the masses of the individual Plummer distributions which are laid out according to a specific grid. Therefore, the genome in our genetic algorithm will encode the masses of these Plummer distributions.

For a specific set of Plummer masses, we need to define a way to evaluate how good the corresponding solution is. Since we are working in the strong lensing regime, it is assumed that the gravitational lens system produces multiple images of one or more sources. If one would project these images back to the source plane using the exact lens equation for the lens under study, one would find that back-projected images of the same source will overlap perfectly. For this reason, the degree in

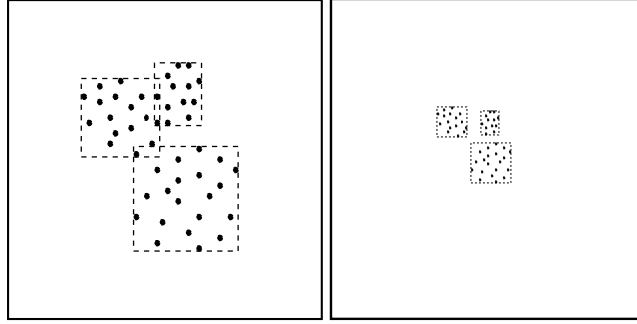


**Figure 2.** Evaluating the fitness of back-projected images. In the left panel, on an absolute scale, the value of the potential energy of the imaginary springs connecting the rectangles that enclose the back-projected images of a single source is higher than in the situation depicted in the right panel. However, the back-projected images in the left panel overlap, unlike those in the right panel. We therefore scale the rectangles enclosing the back-projected images of a single source with the mean size of the rectangles when calculating the fitness value.

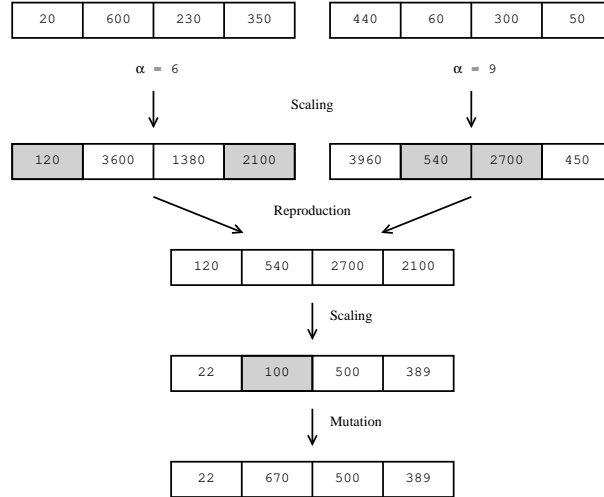


**Figure 3.** Reproduction and mutation of genomes. See text (subsection 3.2.2) for explanation.

which back-projected images of the same source overlap will be used to determine how good the suggested solution actually is.

The way this is implemented is as follows. For a given solution of the mass distribution of the lens, the images of a single source are projected back to the source plane. The areas occupied by each image are surrounded by rectangles: two examples are shown in Fig. 2. Corresponding corners of the rectangles are connected with imaginary springs. Consider two rectangles, each enclosing a backprojected image. For corresponding corners, the distance is calculated in absolute units, for example in units of arcminutes or arcseconds. In a previous step, a length scale was calculated as the average of the lengths of the sides of all the rectangles belonging to a specific source. The distance between two corresponding corners is then divided by this length, yielding a dimensionless distance  $d$ . The “potential energy” for this pair of corners is then simply  $d^2$ . Repeating this for the other three corners and adding together the energies then gives the potential energy of these two rectangles. For a specific source, this procedure is then done for all pairs of backprojected images and the sum of these potential energies is then the potential energy contribution of this source. The fitness value of a given lens solution is the sum of the potential energies of all sources. It is important to take into account the scaling of the rectangles when calculating the potential energy values. Comparing the left and right parts of Fig. 2, it is clear that the left situation definitely corresponds to a better overlap, while on an absolute scale the potential energy of the right situation will be the lower one. For this reason, we express distances between corners of rectangles relative to the size of the rectangles, or, in other words, relative to the size of the source.

As was mentioned above, the genome represents the masses of the individual Plummer distributions. To be more precise, the genome only represents the relative contribution of each Plummer distribution: each Plummer mass is represented by a dimensionless, integer number between 0 and 1000. These numbers are stored in the vector  $M$  and the matrix product

$$\Theta' = \gamma M \quad (8)$$

is calculated. For the dimensionless masses to be converted into real masses, the vector  $M$  needs to be multiplied with a factor  $\mu$ , bringing the lens equation in the form

$$B = \Theta - \mu\Theta'. \quad (9)$$

Since  $\Theta$  and  $\Theta'$  are constant column matrices, it is an easy and computationally inexpensive task to find, for a given  $M$ , the factor  $\mu$  that maximises the fitness, or, in other words, for which the back-projected images of the sources coincide best. The value of the fitness of that particular situation is then considered to be the fitness of the genome.

### 3.2.2 Reproduction and mutation

In our implementation, a population of 250 genomes is used. Based on the many simulations we did (see below), 250 genomes has always led to good solutions within an acceptable amount of time. To obtain a new population, some genomes are copied from the original population while others are obtained by merging two genomes. The procedure of merging two genomes consists of a few steps which are illustrated in Fig. 3. At first, the values between 0 and 1000 of each genome are multiplied with their best  $\mu$  value to obtain the true Plummer masses they represent. Then, for each Plummer distribution, the procedure selects at random the mass from one of the two genomes. Finally, these values are rescaled to integer numbers in such a way that the largest number is 500.

When the new population is complete, mutations are introduced in some genomes. In early generations, some values are simply changed to a random number between 0 and 1000. It is for this reason that the previous step rescaled the Plummer masses to a maximum value of 500. This way, a random change of the value will also allow a considerable increase in mass for that Plummer distribution.

When the best fitness values of successive generations start to converge, a new mutation rule is adopted. In this case, random integer numbers in the interval  $[-200, 200]$  are generated and added to some of the genomes' values. Resulting values which are negative or larger than 1000, are set to zero or 1000 respectively. The first mutation rule makes sure that a large range of mass densities can be inspected. When the algorithm starts to converge near a good solution, the second mutation rule assures that the algorithm can more closely approach the best solution.

### 3.2.3 Stopping criterion

The algorithm can be stopped if the fitness of the best genome ceases to improve significantly. We use the following stopping criterion : if the fitness of the last generation, denoted by `new_fit` fulfills the constraint  $|\text{new\_fit} - \text{old\_fit}| < \text{new\_fit}/50$ , with `old_fit` the fitness of 150 generations ago, the algorithm is stopped. We inspected that raising the factor of 50, so that the code runs longer, does not significantly change the solution, i.e. that the solution has converged. Just for safety, we implemented an upper limit of 15000 on the number of generations but all inversions we tried so far converged after less than 5000 generations.

## 3.3 Averaging multiple solutions

The genetic algorithm uses a random initial population, selects genomes at random and introduces random mutations. Because of this, multiple applications of the inversion procedure for a specific set of images will in general yield slightly different solutions. These solutions are all equally acceptable: in all cases, the back-projected images of a single source coincide very well with each other and with the true position of the source. Given this variety of possible solutions, it is interesting to calculate the average of a set of solutions. This averaging procedure will enhance the common characteristics of all the individual lens solutions while suppressing random fluctuations. One can also calculate the standard deviation of these individual solutions. This will identify the regions in which the solutions agree as well as the regions in which there is a lot of uncertainty about the mass density. Averaging the solutions will also increase the smoothness of the retrieved mass density.

What determines the convergence of the fitness value (see section 2.3) is the amplitude of the mutations. Once the difference between the best possible lens solution and the best genome becomes comparable to or smaller than the mutation amplitude, the best genomes of subsequent generations merely scatter around some lowest achieved fitness value. Lowering the mutation amplitude when the fitness starts to converge and averaging a few tens of independent solutions both help to get as close as possible to the best possible solution.

Being able to create an averaged solution is an attractive feature of our approach, but it would be of little use if the resulting mass density would not be a good solution of the inversion problem (or a worse solution than the individual solutions). Using simulations (see Sect. 4), we found that the averaged solution is indeed also a good solution, with a very high fitness, and in many cases even does a better job than many of the individual solutions. This is because the random mutations that occur during the reproduction process of the genomes, cause the best solution to oscillate around the “true” solution. Since averaging a set of solutions suppresses these random fluctuations, the averaged solution can be a more faithful realisation of

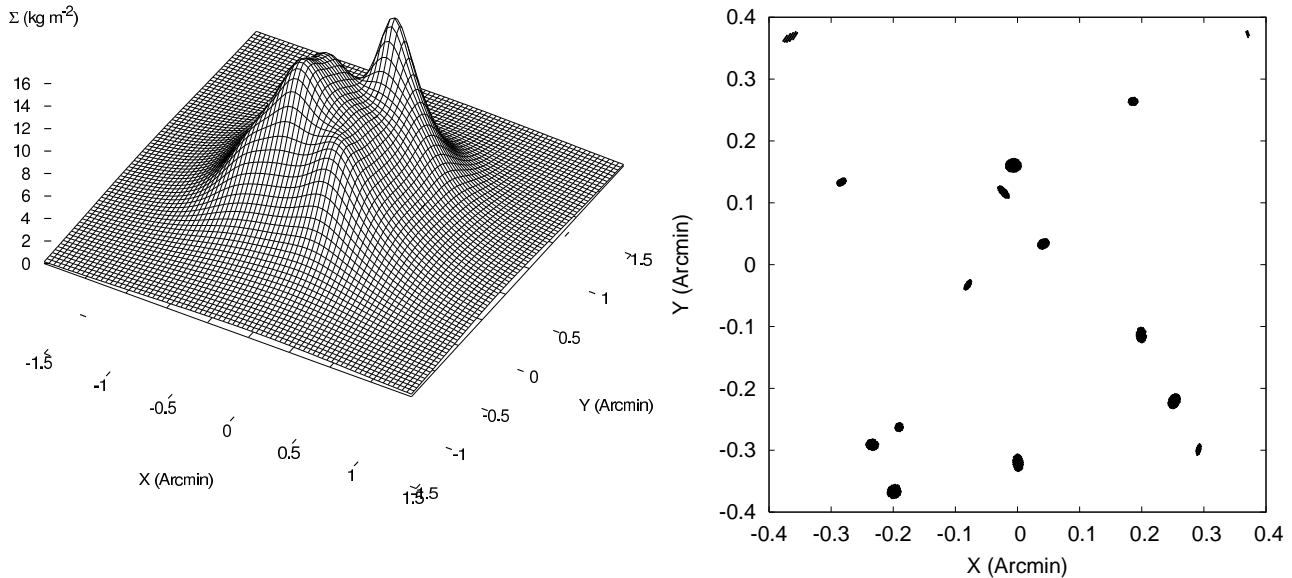


**Figure 4.** Left panel: the mass distribution of the input lens used in the simulation. The total lens mass within a radius of  $1.5'$ , which is slightly further out than the position of the outermost image, is  $0.95 \times 10^{15} M_{\odot}$ . Right panel: the positions and shapes of the 15 sources used in the simulation within the source plane.

the true solution than any of the individual solutions. Also, the inversion of a gravitational lens is clearly an ill-posed problem so it's no great surprise that multiple solutions exist. For these reasons, the averaged solution is definitely a very acceptable one.

#### 4 SIMULATIONS

We conducted many simulations in order to test the validity of our approach. Having full knowledge of the original lens as well as of the original sources, we can easily check the accuracy with which lenses can be reconstructed in ideal circumstances, i.e. when the redshifts of the lens and the sources are known exactly. The mass distributions of the lenses in these simulations were created by randomly adding a number of Plummer distributions. The number of sources, their positions and redshifts were also chosen at random. A wide variety of these gravitational lens systems were used to test the algorithm. In the example that we present below, a lens with mass of the order of  $10^{15} M_{\odot}$  was positioned at  $z = 0.45$  while the redshifts of the sources were sampled from a uniform distribution in the interval  $[1.2, 4.0]$ .

In Fig. 4, we show the mass distribution and the positions and shapes of the sources. The total mass of the lens within a radius of  $1.5'$ , which is slightly further out than the position of the outermost image, is  $0.95 \times 10^{15} M_{\odot}$  and the number of sources in this simulation is 15. This configuration was used to generate the images shown in the left panel of Fig. 5, which in turn serves as input for the inversion algorithm. The resolution of this image is  $1024 \times 1024$  pixels. Critical lines and caustics for a source at redshift  $z = 2.5$  are presented in the right panel of Fig. 5, in which the source positions are also indicated. The genetic algorithm then constructs a lens solution that projects images of a single source onto overlapping regions in the source plane. For this particular simulation, the fitness converged for a grid containing about 400 Plummer mass distributions. As explained before, multiple applications of the inversion algorithm yield different solutions. Still, each solution manages to produce overlapping back-projected images and, while this is in no way enforced by the algorithm, the positions of the back-projected images are very close to the true source positions.

After applying the inversion routine 25 times and averaging the individual solutions, we obtained the final solution presented in the left panel of Fig. 6. This figure shows a striking resemblance to the left panel of Fig. 4. Clearly, the mass distribution of the lens is retrieved with very high accuracy. The fitness values of the 25 individual solutions and of the averaged solution are shown in the left panel of Fig. 7. Since averaging the individual solutions suppresses random generation-to-generation fluctuations, which can even prevent the solutions from further lowering the fitness value, and enhances their common traits, the averaged solution outperforms each individual solution. When the images of Fig. 5 are projected back onto the source plane, we obtain the situation shown in the right panel of Fig. 6. The back-projected images overlap very well and are close to the true source positions. The critical lines and caustics of the averaged solution for a source at redshift  $z = 2.5$  are shown in the right panel of Fig. 7, which can be compared with the right panel of Fig. 5. Again, the resemblance is striking.

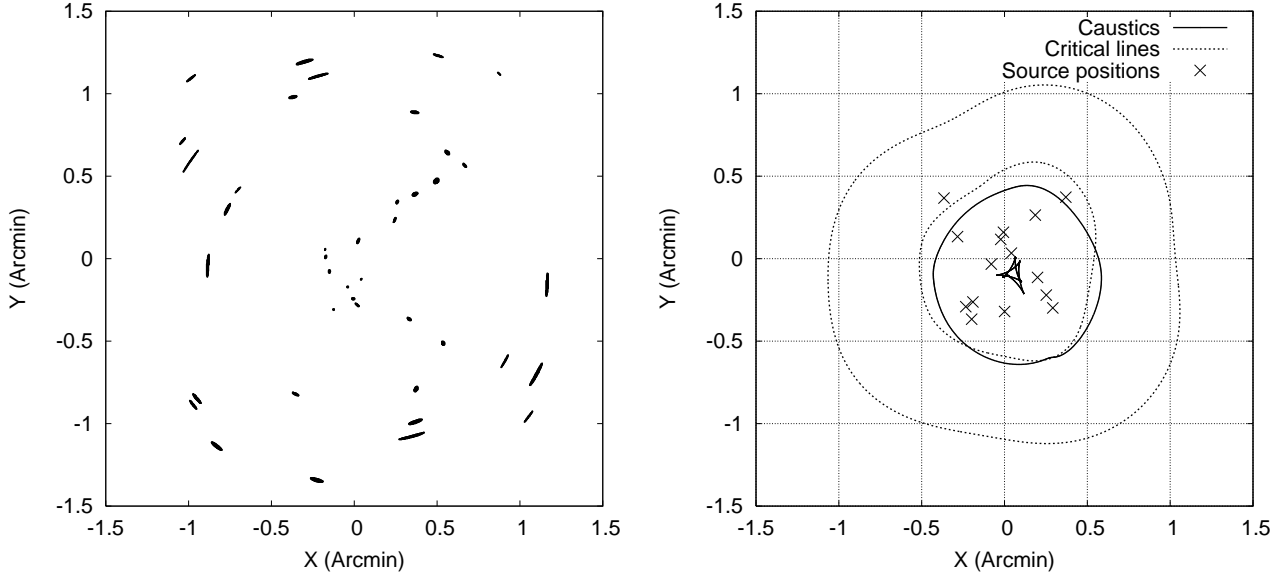


**Figure 5.** Left panel: the image used as input for the inversion routine in the simulation. The resolution of this image is  $1024 \times 1024$  pixels. Right panel: the critical lines (dotted lines) and caustics (full lines) of the lens for a source at redshift  $z = 2.5$ . The crosses indicate the positions of the sources.

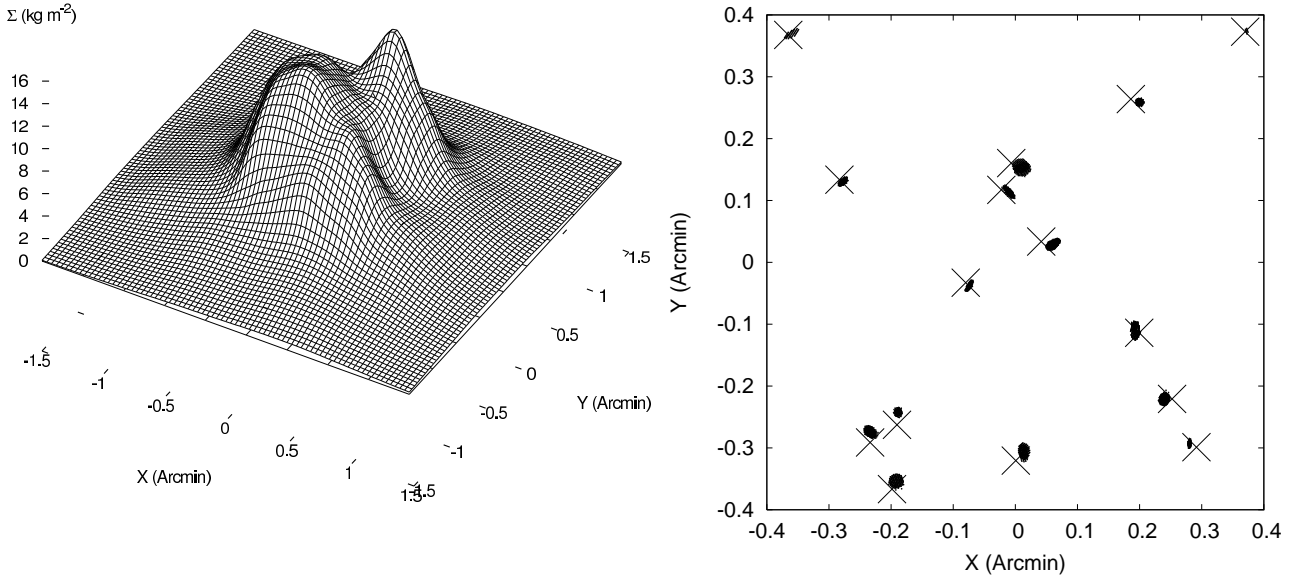


**Figure 6.** Left panel: the average of 25 individual solutions for the simulation. The total mass of this averaged lens solution within a radius of  $1.5'$  is  $0.96 \times 10^{15} M_{\odot}$ . This figure can be compared with the left panel of Fig. 4. Right panel: the positions of the back-projected images within the source plane for the averaged solution of the simulation. The true source positions are marked with crosses. This figure can be compared with the right panel of Fig. 4.

In the left panel of Fig. 8, we show the absolute value of the difference between the mass distributions of the input lens and of the averaged solution. In the right panel of Fig. 8, the standard deviation of the 25 individual solutions is presented. The first quantity is a measure for the quality of the fit, the second measures the disagreement between the individual solutions.

For a circularly symmetric lens, only the total mass enclosed within the radius of the outermost image can be determined. The lens employed in the simulation is not spherically symmetric but one can still surmise that we do not have a very good handle on the mass outside the outermost image. In Fig. 9, we show the circularly averaged density profiles of the input lens and of the averaged solution. As expected, both agree excellently with each other within the inner  $\sim 1.5'$ , which is about the



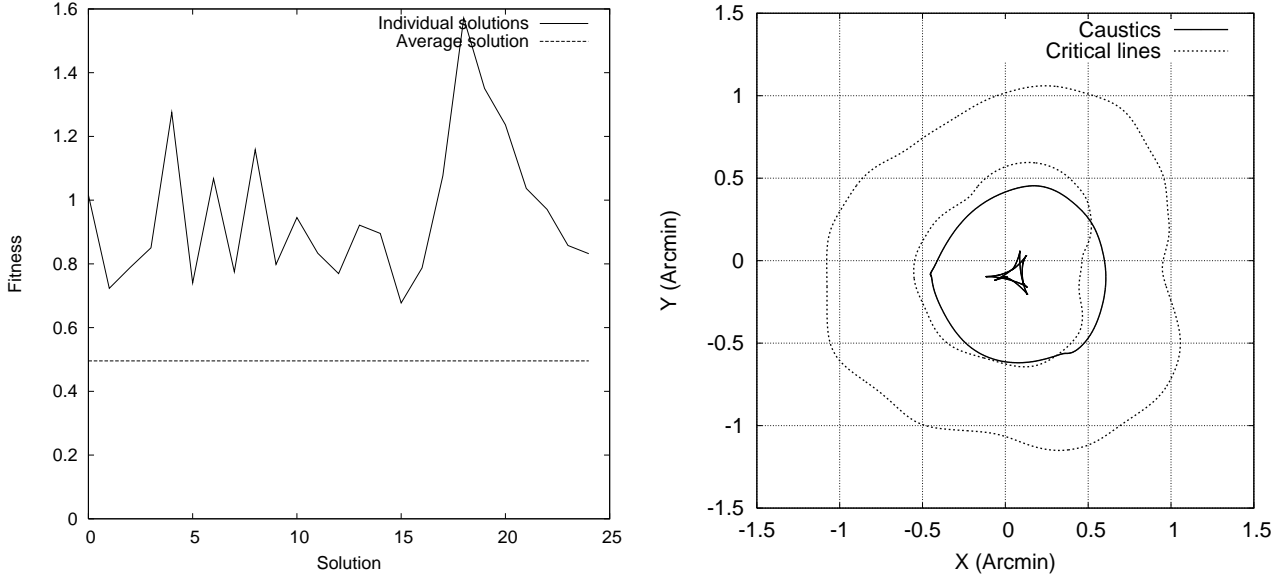


**Figure 7.** Left panel: the fitness values of the 25 individual solutions compared with the fitness value of the averaged solution for the simulation. The averaged solution is clearly superior to the individual reconstructions. Right panel: the critical lines and caustics for a source at redshift  $z = 2.5$  of the averaged solution in the simulation. This figure can be compared with the right panel of Fig. 5.

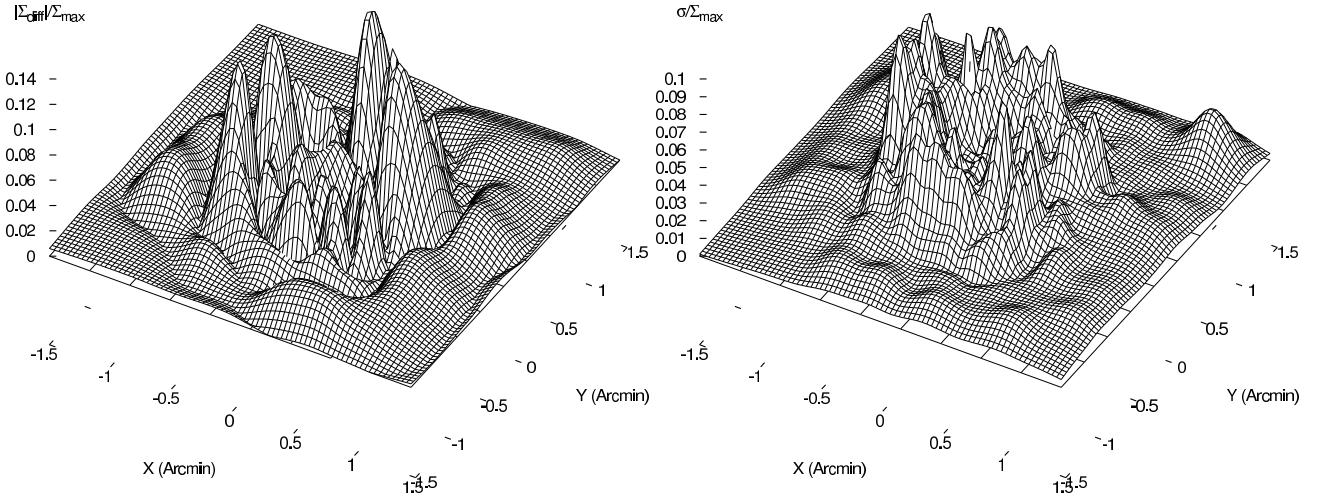


**Figure 8.** Left panel: the absolute value of the difference between the mass distributions of the input lens and of the averaged solution of the simulation, relative to the maximum mass density of the input lens. Right panel: the standard deviation of the 25 individual solutions of the simulation, relative to the maximum mass density of the input lens.

position of the outermost image. Outside that radius, the density is no longer well constrained by the data and the profile of the best lens solution drops below that of the input lens. For the averaged solution, the mass enclosed within a radius of  $1.5'$  is  $0.96 \times 10^{15} M_{\odot}$  which can be compared with the input lens, which comprises a mass of  $0.95 \times 10^{15} M_{\odot}$  within the same radius.

From this simulation and the many others we have ran, we conclude that given enough observational constraints, our method succeeds in inferring the mass distribution of a lens given the redshifts of the lens and the sources and the positions and shapes of the images. If the sources sample the caustics sufficiently well, the density profile of the lens can be reconstructed with great accuracy out to the outermost image. A very important feature of our method is that it does not minimise residuals of the lens equation, like e.g. SLAP. Because tangential images are larger than radial ones, this residual is dominated by the tangential arcs and, as a consequence, methods that make use of it are less sensitive to the information contained in the radial images. This is clear from e.g. Diego et al. (2005b), where the non-parametrically reconstructed density profile of the cluster

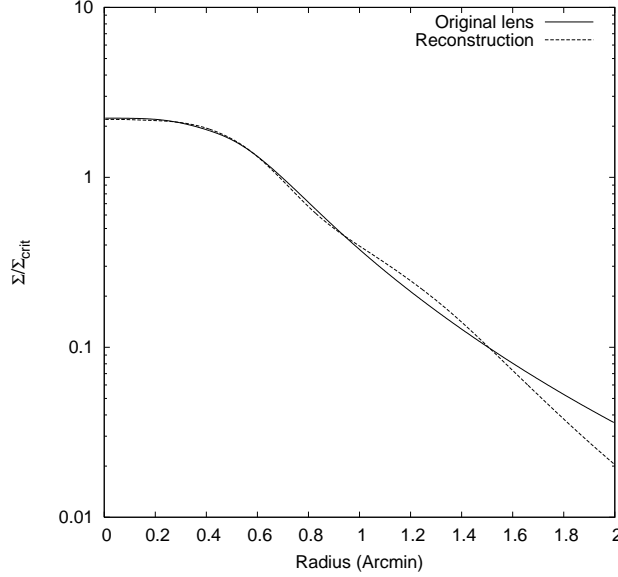


**Figure 9.** The circularly averaged density profiles of the input lens (full line) and of the averaged solution (dotted line), normalized to the critical density for a source at redshift  $z = 2.5$ . Within a radius of  $1.5'$ , which coincides with the position of the outermost image, both profiles agree very well. Outside this radius, the density of the averaged solution is not constrained very well by the data and drops below that of the input lens.

A1689 shows a central decline which the authors contribute to this effect. Our method is insensitive to the size of the images and thus makes full use of the information contained in the radial images. This is reflected in Fig. 9, which shows that the central density of the input lens is very accurately retrieved.

## 5 DISCUSSION AND CONCLUSION

The procedure described and illustrated above is a non-parametric method for inverting gravitational lenses, making no a priori assumptions regarding the shape of the lens. We only impose the condition that an acceptable solution must be able to map images of the same source onto overlapping regions in the source plane. The procedure only requires that one can identify which images correspond to the same source. In particular, no information about the sizes of the sources needs to be provided. The size of the grid on which the algorithm will determine the mass distribution of the lens needs to be specified. However, because a single solution can be obtained relatively fast, it is an easy task to try a variety of sizes until one is obtained which generates a lens with a good fitness value. A multi-resolution grid with a few hundred cells is usually sufficient to represent any plausible lens mass distribution. The implementation used for the simulation in this paper employs a population of 250 genomes. Based on a suite of simulations, this value proved to be sufficiently large to yield good solutions within an acceptable amount of time. The calculations were done in a distributed manner, using sixteen Intel® Xeon™ 2.4 GHz processors of a computer cluster. Depending on the number of sources, creating a single solution may require several hours. To give a specific example, the 25 solutions used in the simulation were created in four days.

The simulation discussed in this article, together with the many others we performed, indicate that our inversion technique successfully solves the lens inversion problem. The reconstructed sources lie close to their true positions and their shapes are retrieved quite accurately as well. The procedure determines the mass of the lens very accurately. The averaging procedure guarantees the removal of random fluctuations and yields a smooth mass density very close to the true solution. Note that because the masses of the individual Plummer distributions are always represented by positive numbers in the genome, no negative mass densities will be produced.

Of course, the quality of the reconstruction depends on the quality of the information at hand. The algorithm depends on the availability of multiply imaged sources, which identifies the relevant area in our procedure as the area within the outermost caustic. When this area is sampled well by the sources, we can expect a good reconstruction of the mass density, as indicated by the simulation described previously. A major advantage of the algorithm is that it makes full use of the information contained in the radial images, unlike methods that minimise the residuals of the lens equation, and is thus able to accurately reconstruct also the inner parts of the lens.

Another advantage of a genetic algorithm is the ease with which the fitness criterion can be specified. One simply has to devise a way to associate a fitness value with a specific genome, without worrying about features like continuity or

differentiability. E.g., to test whether information about the amplifying effect of the gravitational lens can improve the lens reconstruction, we added a contribution to the fitness value: the maximum brightness values in the back-projected images of a single source should lie as close as possible to each other. Several simulations indicated that augmenting the procedure in this fashion does not improve the final result since the  $\beta(\theta)$  mapping was already very well approximated anyway. Not requiring surface brightness information not only reduces the computational cost, but also makes the method less sensitive to noise in the images. Incorporating information about the shear field at larger radii outside the gravitational lens is straightforward. For each genome the shear components  $\gamma_1(\theta)$  and  $\gamma_2(\theta)$  can be calculated and compared with the observed values. The expression for the fitness can be changed so as to penalise genomes with large differences between the measured and the model shear. Further improvements of the genetic algorithm, such as making the mutation amplitude depend automatically on the convergence of the fitness, are easily implemented and are left as future research. An application to real data will be presented in a subsequent paper.

## ACKNOWLEDGMENTS

We would like to thank Prof. Philippe Bekaert and Tom Van Laerhoven of the Expertise Centre for Digital Media for granting us access to the computer cluster and for taking care of the related practical issues. We also would like to thank the anonymous referee for the valuable remarks and suggestions. They very much improved the content and presentation of this paper.

## REFERENCES

- AbdelSalam, H. M., Saha, P., Williams, L. L. R., 1998, MNRAS, 294, 734  
 Bradač, M., Erben, T., Schneider, P., Hildebrandt, H., Lombardi, M., Schirmer, M., Miralles, J.-M., Clowe, D., Schindler, S., 2005, A&A, 437, 49  
 Broadhurst, T., Benítez, N., Coe, D., Sharon, K., Zekser, K., White, R., Ford, H., Bouwens, R. et al., 2005, ApJ, 621, 53  
 Brewer, B. J. & Lewis, G. F., 2005, PASA, 22, 128  
 Diego, J. M., Protopapas, P., Sandvik, H. B., Tegmark, M., 2005, MNRAS, 360, 477  
 Diego, J.M. Sandvik, H.B., Protopapas, P., Tegmark, M., Benitez, N., Broadhurst, T., 2005, MNRAS, 362, 1247  
 Diego, J. M., Tegmark, M., Protopapas, P., Sandvik, H. B., 2005, submitted to MNRAS (astro-ph/0509103)  
 Diemand, J., Moore, B., Stadel, J., 2004, MNRAS, 353, 624  
 Dyer, C. C. & Roeder, R. C., 1980, ApJ, 238, 67  
 King, L. J., Clowe, D. I., Schneider, P., 2002, A&A, 383, 118  
 Kneib, J. P., Mellier, Y., Fort, B., Mathez, G., 1993, A&A, 273, 367  
 Kochanek, C. S., Blandford, R. D., Lawrence, C. R., Narayan, R., 1989, MNRAS, 238, 43  
 Koza J. R., 1992, Genetic Programming: On the Programming of Computers by Means of Natural Selection. MIT Press, Cambridge, MA, USA  
 Lavery, R. J. & Henry, J. P., 1988, ApJ, 329, 21  
 Liebes, S., 1964, Phys. Rev., 133, 835  
 Meneghetti, M., Jain, B., Bartelmann, M., Dolag, K., 2005, MNRAS, 362, 1301  
 Navarro, J. F., Hayashi, E., Power, C., Jenkins, A. R., Frenk, C. S., White, S. D. M., Springel, V., Stadel, J., Quinn, T. R., 2004, MNRAS, 349, 1039  
 Plummer, H. C., 1911, MNRAS, 71, 460  
 Refsdal, S., 1964, MNRAS, 128, 295  
 Saha, P. & Williams, L. L. R., 1997, MNRAS, 292, 148  
 Soucail, G., Fort, B., Mellier, Y., Picat, J. P., 1987, A&A, 172, 14  
 Soucail, G., Kneib, J.-P., Golse, G., 2004, A&A, 417, L33  
 Trotter, C. A., Winn, J. N., Hewitt, J. N., 2000, ApJ, 535, 671  
 Tyson, J. A., Kochanski, G. P., Dell’Antonio, I. P., 1998, ApJ, 498, L107  
 Wallington, S., Narayan, R., Kochanek, C. S., 1994, ApJ, 426, 60  
 Yamamoto, K., Kadoya, Y., Murata, T., Futamase, T., 2001, P. Th. Ph., 106, 917